Chapter 2
Theory

This chapter will give a brief introduction to the most relevant theoretical aspects used in this thesis, with the aim of explaining the most important formulae and ideas. We will start with basic theory of electrons in metals. Moving on from free electron theory we will give the outline to a more realistic theory for our experimental results. We will then describe the theory of quantum oscillations, which is necessary to understand the main results of this thesis. We will then turn to a brief introduction to the fundamental superconducting properties that we will need in the discussion and interpretation of experimental results. One of the main aspects of this thesis is the quantum critical system $BaFe_2(As_{1-x}P_x)_2$. Also in the cuprate superconductor quantum criticality is often discussed as possible origin of high temperature superconductivity. A brief introduction to the topic of quantum criticality shall therefore be given from the starting point of classical phase transition.

2.1 From Free to Nearly Free Electrons

We begin by a brief introduction following the historical development that led to our current understanding of the behaviour of electrons in metals that will be given in the next section. While a first model proposed by Drude treated the electrons as a classical *free electron gas*, we will start by modelling the electrons in a solid as *free electron gas* in a one dimensional potential considering electrons as waves rather than particles. This *ansatz* was first proposed by Sommerfeld and Bethe. Solving the time-independent Schrödinger equation for this system we find standing waves whose energies are equivalent to those of a free electron but with discrete wave-numbers k. In three dimensions a constant energy in reciprocal space is represented by a sphere that contains a certain number of discrete k-states. The density of states can then be determined from the number of states per energy interval. This leads to the relation $D(E) \propto m^{3/2}E^{1/2}$ for the density of states in three dimensions, which holds as long as we consider a non-interacting single electron picture.

C.M. Putzke, *Fermi Surface and Quantum Critical Phenomena in High-Temperature Superconductors*, Springer Theses,
DOI 10.1007/978-3-319-48646-8_2

The distribution $f(T, E)$ of electrons among the available states is determined by the temperature of the system. The density of electrons is given by

$$n = \int_0^\infty D(E) f(T, E) dE. \tag{2.1}$$

Since electrons are Fermions (spin 1/2), we need to use the Fermi-Dirac distribution function

$$f(T, E) = \frac{1}{e^{(E-\mu)/k_B T} + 1}, \tag{2.2}$$

with the chemical potential μ of the system and the Boltzmann-constant k_B and the Pauli exclusion principle. Form this we find that at $T = 0$ all electrons populate the lower energy states up to the chemical potential μ. The sphere of constant energy $E_F = \mu$ in k-space that contains all these states is known as the *Fermi-surface*, and the energy E_F as *Fermi-energy*.

This simple model of the electrons in a solid produced for the first time the correct interpretation of the heat capacity of simple metals like copper, where a linear dependence of the electronic specific heat in temperature was found. However we would not be able to understand the origin of metallic, semi-conducting or insulating behaviour in this context. Hence the assumptions made can only give a crude understanding of the system. In the further course of this work we will now try to reduce these assumptions of a constant background potential (*nearly free electron*), non-interaction (*Fermi-liquid theory*) and one-electron treatment (*density functional theory*) step by step to try to obtain a better understanding of the complex nature of electrons in solids.

2.1.1 Nearly Free Electron

A more realistic scenario for the background potential in a solid is the use of a periodic potential. The potential represents the Coulomb potential of the ionic lattice. We further include the Born-Oppenheimer approximation in our treatment. In this the electrons respond immediately to any lattice vibration as their typical velocity is orders of magnitude higher than that of the lattice. Therefore the lattice potential is given as mean field result, typically represented by the equilibrium state. The electrons in this scenario are split. While low energy electrons are bound to the ions, reducing the Coulomb potential by shielding, the so called *valence electrons* are free to move without any other interaction than those with the lattice potential. From symmetry arguments the solutions $\psi_k(r)$ of the time-independent Schrödinger equation is now represented by a plane-waves modulated by a factor $u_k(r)$ periodic on the lattice, meaning $u_k(r) = u_k(r + r_n)$, with the lattice periodicity r_n. The resulting single-electron solutions

$$\psi_k(r) = u_k(r)e^{ikr} \tag{2.3}$$

are known as *Bloch-waves*. In reciprocal space we find that the potential is periodic with the vector G, so that $\psi_{k+G}(r) = \psi_k(r)$ and hence $E(k) = E(k + G)$. This shows that the single particle energy $E(k)$ is periodic in reciprocal space and hence in further treatment we only need to consider the first Brillouin-zone (BZ).

We will now consider the dispersion $E(k)$ for a very weak potential, meaning that we first only consider the periodicity, leaving the strength of the potential negligible. In this case we find the dispersion relation $E(k)$ for a free electron periodically spaced in reciprocal space as shown in Fig. 2.1a. At the BZ boundaries the energies $E(k)$ are degenerate. In quantum mechanics this leads to the superposition of the two plane waves. Now we add the magnitude of the periodic potential. The two superimposed plane waves will have different energies resulting from a phase difference. This leads to the lifting of the degeneracy of $E(k)$ and a splitting of the energies at the crossing points. This is schematically shown in Fig. 2.1c. Therefore we find now that electrons in the presence of a periodic potential do not possess a continuous energy spectrum. This we know as the *band structure* of a solid. With this we can also understand the origin of metallic and insulating behaviour. If the Fermi energy is located in between bands then the available bands are filled and we need to overcome the energy-gap to the next band in order to excite electrons. In the case where the Fermi energy lies within a band this is not the case and a continuous increase in energy will lead immediately to excited electrons.

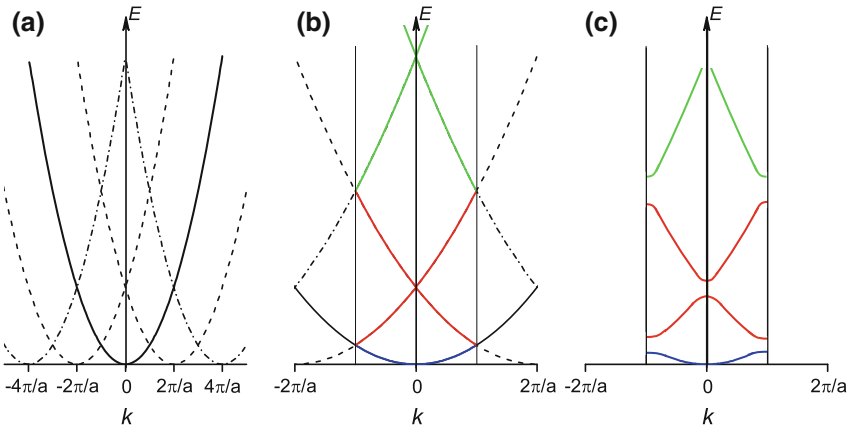

Fig. 2.1 Dispersion relation $E(k)$ for (**a**) a free electron model (**b**) for an infinitesimal small periodic potential and (**c**) a periodic background potential leading to the band structure in *solids*

2.2 Fermi-Liquid Theory

In the next step towards our understanding of electrons in metals we want to include interactions of electrons. For this we will turn to *Fermi liquid theory* (FL). This theory developed by Landau [1] for *neutral* Fermions was originally motivated to describe the rare isotope of Helium ^{3}He. Fermi liquid theory has been a powerful tool as it correctly describes properties such as the quadratic temperature dependence of the resistivity at low temperatures and the temperature dependence of the susceptibility. Today however most novel phenomena are concerned with the emergence of non-Fermi liquid like behaviour such as one-dimensional systems, or systems that are tuned close to a quantum critical point where the approximation of weak interacting Fermions does not hold any more. We find this non-Fermi liquid behaviour, typically characterized by $\rho \propto T$ in systems like the iron-pnictides and cuprates studied in this work [2–4]. However lacking a theory with the same predictive power as the Fermi liquid theory, especially close to quantum critical points, we try to understand these materials based on how they deviate from the conventional prediction by FL theory.

In order to implement interactions to the free-electron model we start by assuming the distribution function $n_0(\mathbf{k}, \sigma)$ of the non-interacting system. When introducing the interactions to this non-interacting system we have to keep in mind that any excitation will only possess a certain life-time τ after which the system will relax. However we need to turn on the excitations *adiabatically* such that the same distribution function also describes the interacting system. This leads to the limitation that the life-time τ in the system needs to be sufficiently long such that they are longer than the adiabatic introduction of excitations. This limits the theory to describe *weak* interactions that produce excited states close to the Fermi level.

As we are interested in electrons in a solid we use the Fermi distribution at T=0 for our non-interacting system. Hence all occupied states take the value $n_0(k, \sigma) = 1$ and all others are zero. The *adiabatic* introduction of interactions to the system, has two further consequences. While the distribution $n(k, \sigma)$ of the new *quasiparticle* is given by the same form as $n_0(\mathbf{k}, \sigma)$ at $T = 0$, the eigenstates are superpositions of the original non-interacting eigenstates. The difference between the distribution of free-electrons and quasiparticles and that of electrons in a Fermi liquid is shown in Fig. 2.2 [5]. While the quasiparticles, as required have the same distribution as the

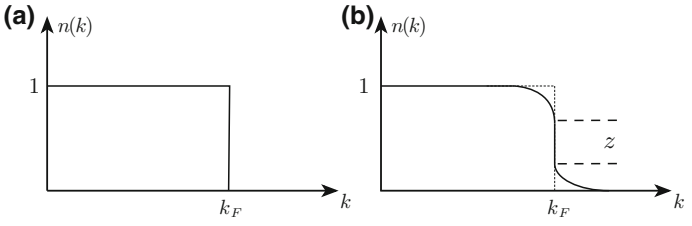

Fig. 2.2 Probability distribution n for a state k to be occupied at T=0. **a** For a non-interacting electron system, or quasiparticles in a Fermi liquid and **b** for electrons in an interacting Fermi liquid

free electron system, the interacting electrons in the Fermi liquid show a reduced step at the Fermi level. The remaining step causes the picture of a Fermi surface to remain valid in the case of an interacting system and the size of the jump Z is inversely proportional to the *effective mass* of the quasiparticles.

From the concept of quasiparticles, which form the basis of this theory, we can now understand why the *free-electron theory* was so powerful in its predictions. The quasiparticles, describing the interacting system, are thought of as non-interacting gas, where the collective interactions of the system are represented by changes in characteristic parameters such as the quasiparticle mass. This however will not change the qualitative results of the temperature dependence of for example the specific heat, but only their absolute magnitude. Further it allows us, within the approximation of a weakly interacting system, to map the problem of collective interaction on a non-interacting single particle wave-function.

We now consider what happens to the energy ε of the system when we add one quasiparticle. For weak interactions we assume a linear dispersion around ε_F, which leads to the new energy of the system [5]

$$\varepsilon_p = \varepsilon_F + \frac{p_F(\hbar k - p_F)}{2m^*}, \tag{2.4}$$

with the Fermi momentum p_F. Here we assume that the Fermi wave vector k_F is unchanged from the non-interaction system. The velocity of the quasiparticle is given by the energy-momentum derivative

$$\upsilon = \frac{d\varepsilon}{dp} = \frac{p_F}{m^*} = \frac{m}{m^*}\upsilon_F. \tag{2.5}$$

This shows that the group velocity of the quasiparticle, which is modified due to interactions, is modified by the ratio of the bare electron mass to the mass m^* known as *effective mass* or *quasiparticle mass*.

So far we have only considered a single quasiparticle neglecting any contribution of interaction to the total energy. The energy dispersion including exchange interactions is given as [6]

$$\varepsilon = \varepsilon_F + \frac{p_F(\hbar k - p_F)}{m^*} + \sum_{k,\sigma} f_{k\sigma,k'\sigma'}\delta n_{k'\sigma'}, \tag{2.6}$$

where $\delta n_{k'\sigma'}$ represent changes in the particle distribution and $f_{k\sigma,k'\sigma'}$ are a second phenomenological parameter known as *Landau interaction function*. Commonly in textbooks the properties of the Fermi-liquid are described by the so called *Landau-parameter* $F_l^{a,s}$, which can be derived from $f_{k\sigma k'\sigma'}$ [7].

Both m^* and f are not independent of each other. Using the *Landau-parameter* we can express the effective mass as [7]

$$\frac{m^*}{m} = 1 + F_1^s. \tag{2.7}$$

Here the superscript s represents *spin symmetric interaction*. From this we find that in the case where quasiparticle interaction become too strong, for example on approaching an ordered state, the effective mass will diverge. The fact that even in heavy fermion materials effective masses of $m^* \approx 1000$ were found to be in good agreement with measurements of Sommerfeld coefficient γ, shows the wide variety of possible applications.

We want to point out that the parameters m^* and $F_l^{a,s}$ are phenomenological values that need to be experimentally determined. The power of Fermi liquid theory does not rely in predicting experimental results, but rather helps finding the hallmarks of strongly correlated effects in solid state physics. It also allows further inside by linking experimental results on different properties such as heat capacity, magnetic susceptibility and quantum oscillations.

2.3 Density Functional Theory

At this point we have developed an understanding of relative behaviour of experimental values and their origin within the properties of electrons in system using the nearly free electron picture. By adding Fermi liquid theory we are further able to understand the origin of different absolute behaviour of physical properties, such as the Sommerfeld coefficient, between different materials. We have seen that we can explain the interacting Fermi liquid as Fermi gas of quasiparticles, where the interactions are taken into account by only two intertwined parameters, the quasiparticle mass m^* and the Landau parameter $F_l^{a,s}$. However these are so far of phenomenological nature and need to be experimentally determined. For a better understanding of the evolution of correlated electron systems, it would be desirable to be able to predict these values theoretically. For this the *density functional theory* is a powerful tool.

The *density functional theory* (DFT) gets its name from the Hohenberg-Kohn theorem. This states that the ground state energy is a unique functional of the ground state density [6]. So far we had assumed plane waves or in the picture of nearly free electron system Bloch-waves. However we don't know what the ground state wave-function of the real electron-system looks like. Therefore here the transition is made from the ground state wave function to the function of electron-density at place r. Using the *Ritz method* one can then write the ground state energy of the system

$$E_0 = E\{n_0(r)\} \leq \langle \psi | H | \psi \rangle, \tag{2.8}$$

with the ground state density $n_0(r)$ and the ground state of the system $|\psi\rangle$. This could theoretically be used to find the exact ground state by variation of $\delta E\{n(r)\} = 0$. DFT hence offers us the possibility to predict the ground state energy of a system and compare it to experimental findings.

In reality this is not straight forward as the functionals of the kinetic energy $T\{n(r)\}$, the potential energy $V\{n(r)\}$ and the interaction $U\{n(r)\}$, that make up E,

are unknown. While $V\{n(r)\}$ can be assumed to follow the single particle potential as we used in nearly free electron theory, the kinetic functional remains unknown and the interaction functional can only be estimated to the electrostatic exchange plus a term $E_{ex}\{n(r)\}$, the exchange interaction [6].

Kohn and Sham proposed to solve the problem by writing the energy again as a functional of a single particle wave functions $\psi_i(r)$ using [6]

$$n(r) = \sum_{i=1}^{N_e} |\psi_i(r)|^2. \tag{2.9}$$

This leads to the *Kohn-Sham equations* which can be used iteratively to get a solution of the kinetic energy functional. The assumption to use a single particle wave function leads to the fact that the use of the kinetic energy and single particle potential leads still to an exact solution of the many body problem. The reason that the use of a single particle wave-function is applicable lays again in the concept of quasiparticles which we can describe in this way. The interactions are then described by their band mass, enhanced over the free electron mass. On the other hand this limits application to weakly coupled systems. All aspects of the many body problem are now contained in the exchange interaction $E_{ex}\{n(r)\}$, whose form is unknown. We therefore have the same problem as in Fermi liquid theory where the form of the Landau-parameter was not unknown.

As mentioned, the DFT formalism is theoretically exact, but in order proceed we need to make some approximations and hence the results obtained by calculations can only be as good as the validity of the approximation to the real system. The typical approaches to find $E_{ex}\{n(r)\}$ involves the *local density approximation* (LDA) where E_{ex} at place r only depends on the density n at point r or the *generalized gradient approximation* (GGA) that involves in addition to the density at point r, the gradient $\partial n/\partial r$. Both methods are limited to static exchange and correlation effects that are approximated locally. It hence leads to a band structure that lacks long range and fluctuating interactions as well as strong coupling. For this more advanced theories such as *dynamic mean field theory* (DMFT) are necessary. Typically the theoretically determined values of band structure and derived mass, *band mass*, are compared to experimental results. The comparison then holds information whether the local approximation describes the system well or if additional effects need to be taken into account.

DFT calculations have been successfully used in weakly correlated systems such as sodium. In strongly correlated systems however it has its limits, for example in the cuprate-superconductors where it predicts a metallic behaviour while experiments have found insulating behaviour in the parent compounds. The reason for this can be best described when we turn back to Fermi liquid picture. The use of a single-particle description, as present in the Kohn-Sham equations, is a good approach as long as we can define the quasiparticles as free electron gas. This treatment is correct when the spectral weight $E(k, \omega)$ is well represented by strong peaks as seen in Fig. 2.3a for a non-interacting, or (b) for a weakly interacting system as described by

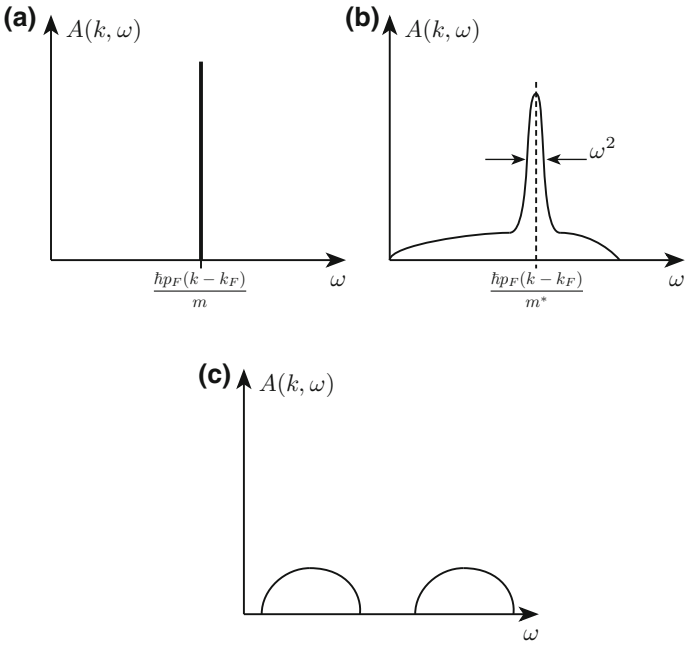

Fig. 2.3 Spectral function $A(k, \omega)$, gives the probability of an electron with momentum k to be found with a given energy ω. **a** For a non-interacting electron the probability is a delta-function, **b** for a Fermi liquid, where the quasiparticles are superimposed of non-interacting states, the peak is smeared out and **c** for a strongly correlated system, like Mott-Hubbard insulators, where the weakly coupled treatment breaks down and no quasiparticle peak is found

Fermi liquid theory. The stronger the interactions become, the more eigenstates of the non-interacting eigenstates need to be taken into account, which leads to enhanced broadening or even a shift of the spectral weight as shown in Fig. 2.3c which is typically found in Mott-Hubbard physics where strong Coulomb repulsion U needs to be taken into account. In this case the system is no longer well described by a LDA.

2.4 Bandstructure Calculations

The following section shall give a brief introduction to the basis of band structure calculations as performed in this work and the most common terms found within. The aim is to sketch the process rather than a detailed theoretical description. A more detailed treatment can be found in Ref. [6, 8].

2.4.1 LAPW

The *linear augmented plane wave* (LAPW) is a combination of the *Wigner-Seitz-method* which assumes spherical harmonics for the wave functions of the atoms and the *plane wave method* which is based on the solution of the Schrödinger equation using Bloch-functions. While the first method proves to be inaccurate in the region between atoms the second is challenging when trying to describe the atomic orbitals, as it requires higher order terms. The way around this is to split the Wigner-Seitz cell in two parts. For the inner part of radius R we assume a spherical potential, while for $r > R$ a constant potential us used. Due to its shape, the resulting potential is known as *muffin tin potential*. For the solution of the Schrödinger equation one uses linear combinations of the form

$$\psi_\varepsilon(r) = \sum_{l,m} A_{l,m} Y_{l,m}(\vartheta, \varphi)\chi_{l,\varepsilon}(r), \tag{2.10}$$

for $r < R$. $Y_{l,m}(\vartheta, \varphi)$ and $\chi_{l,\varepsilon}(r)$ are spherical and radial part of the wave functions and $A_{l,m}$ are Bloch-coefficients. In the region where $r > R$ plane-waves of the from

$$\phi_k(r) = e^{ikr} \tag{2.11}$$

are used. The dispersion relation $\varepsilon(k)$ is then achieved by the condition $\psi_\varepsilon(R) = \phi_k(R)$.

2.4.2 WIEN2k

In this work the WIEN2k package [9] was used for bandstructure calculations in the iron-based superconductors. Within this package the functions described in LAPW are used as basis set for the Kohn-Sham equations within the DFT algorithm. The calculation then follow the Ritz method to minimize the differential with respect to the linear combinations of augment plane waves. In order to estimate the exchange interaction the LDA or GGA approach can be used. The used procedure follows the outline:

1. start with a guess of the density $n_0(\mathbf{r})$
2. determine the single-particle potential from $n_i(\mathbf{r})$
3. application of LDA or GGA to determine the exchange correlation function $E_{ex}(n_i)$
4. solving the Kohn-Sham Equation $H_{KS}\psi = \varepsilon\psi$
5. determine the new density $n_{i+1}((r))$ from ψ
6. if $n_{i+1} \neq n_i$ start over with n_{i+1} as input if not we have have found ground-state density and energy

2.4.3 Dynamic Mean Field Theory

In the course of this work we will compare our experimental results to those obtained by GGA band structure calculations. However there is also a variety of studies in the field of iron-based superconductors that go beyond this approximation and incorporate *dynamic mean field theory* (DMFT) into their calculations [10–12]. DMFT is in these calculations based on LDA calculations. While in LDA we don't make any assumptions on interactions, except of limiting ourself to a local mean field effect, DMFT includes correlations due to Hubbard U and Hund's rule coupling J. These input parameters can more or less be tuned freely and are mostly limited by physical validity.

The choice of input parameter however leads to the fact that we can not see it as a first principle calculation. Also we have to take into account that while systems like the cuprates, where strong onsite Coulomb interaction can be well represented with DMFT [13], the long wave length spin interactions, likely present in the iron-based systems, are not captured in these calculations [11].

2.5 Quantum Oscillation

So far we have focused on the theoretical description of electrons in metals. In this section we will add the magnetic field to this description with the focus on quantum oscillations. In Fermi liquid theory as well as in DFT we have pointed out that we do not possess an exact knowledge of the exchange interaction of electrons in solid. However within Fermi liquid theory we know that those interactions are contained in the Landau parameters. This can be accessed experimentally using the temperature dependence of quantum oscillation amplitude and are determined as effective masses.

Using quantum oscillations in combination with LDA calculations we can further find a theoretical model of the Fermi surface topology that can help us understand electronic correlations in the system.

Within this study we will determine how the effective mass is enhanced over the free electron mass. We should bear that the band mass can refer to different theories and so we need to point out that throughout the context of this work we will use band mass m_b as the mass that has been determined by LDA calculations and hence already includes on-site interactions, at the mean-field level.

We will begin with a semi-classical treatment and then include quantum mechanics to reach the *Lifshitz-Kosevich formula* that describes the *de Haas-van Alphen effect* and lets us extract the relevant information from our experimental results.

2.5.1 Semi-classical Electron in a Magnetic Field

Lets start by considering a free electron in a uniform magnetic field. The motion of the electron will be governed by the Lorentz-force

$$\hbar \frac{\mathrm{d}\mathbf{k}}{\mathrm{d}t} = -e\mathbf{v} \times \mathbf{B}. \tag{2.12}$$

$\mathrm{d}\mathbf{k}/\mathrm{d}t$ is only non-zero perpendicular to the magnetic field $\mathbf{B}$ and the velocity of the electron $\mathbf{v}$. The energy of the electron is then constant and its velocity can be expressed as

$$\mathbf{v}(\mathbf{k}) = \frac{1}{\hbar} \nabla_{\mathbf{k}} E(\mathbf{k}). \tag{2.13}$$

From this we conclude that the electrons are bound to orbits in k-space of constant energy perpendicular to $\mathbf{B}$.

The time that is needed for one revolution t_c is given by

$$t_c = \frac{\hbar^2}{eB} \frac{\partial S(E, k_\parallel)}{\partial E}, \tag{2.14}$$

where S is the k-space area of the electron orbit. This is expressed more commonly using the *cyclotron frequency*

$$\omega_c = \frac{2\pi}{t_c} = \frac{eB}{m_c}, \tag{2.15}$$

with the cyclotron mass

$$m_c = \frac{\hbar^2}{2\pi} \frac{\partial S(E, k_\parallel)}{\partial E}. \tag{2.16}$$

In the case of a free electron system $m_c = m_e$.

2.5.2 Quantum Mechanical Description

To describe the electrons in the system in a more precise way, a quantum mechanical treatment is necessary. The motion of the electron in the magnetic field has to satisfy the Bohr-Sommerfeld-condition

$$\oint \mathbf{p}\mathrm{d}\mathbf{q} = 2\pi(r + \gamma)\hbar. \tag{2.17}$$

In this notation r is an integer value, γ a phase which still needs to be determined and $\mathbf{p}$ the canonical moment

$$\mathbf{p} = \hbar\mathbf{k} - e\mathbf{A}, \tag{2.18}$$

with the vector potential $\mathbf{A}$ defined by $\mathbf{B} = (\nabla \times \mathbf{A})$.

By substituting for $\mathbf{p}$ and solving the integral it turns out that the orbits are such, that they enclose integer values of *flux-quanta* $\phi_0 = h/e$. Transferred into k-space the area of the orbits is given by

$$S_\perp(E, k_\parallel) = (r + \gamma)\frac{2\pi B}{\phi_0}, \tag{2.19}$$

which is known as the *Onsager-relation* [14]. It is immediately clear that for constant magnetic field the area $S_\perp$ is constant for all $k_\parallel$. These tubes are the *Landau-tubes* illustrated for a free-electron system in Fig. 2.4.

We are still left to determine the phase γ. This can be done by solving the Schrödinger equation for a free electron in an applied external magnetic field. Assuming the field pointing along the z-direction we obtain for the orbital energy levels

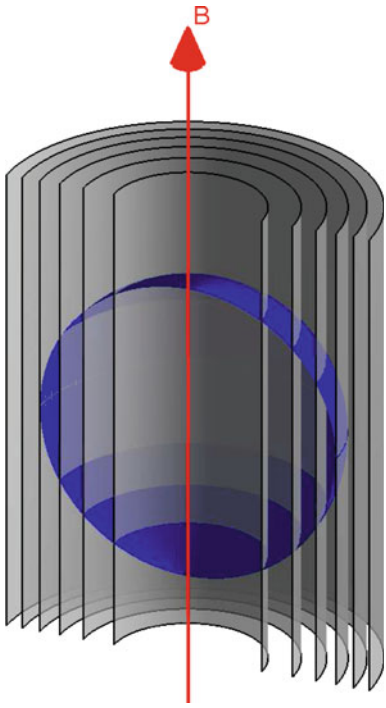

Fig. 2.4 Schematic of *Landau tubes* parallel to the applied magnetic field **B** for a free electron gas with spherical Fermi surface

$$E_n = \left(n + \frac{1}{2}\right)\hbar\omega_c + \frac{\hbar^2}{2m}k_z^2. \tag{2.20}$$

While the energy parallel to the field stays unaffected we again obtain the quantization of energy perpendicular to the magnetic field direction. Comparing this result with the previous and substituting the cyclotron frequency ω_c we obtain the phase $\gamma = 1/2$.

As the size of the orbit changes with field, the Landau-tubes will eventually cross the Fermi-level. The rate at which this happens is determined by the spacing of two consecutive orbits in field

$$\Delta\left(\frac{1}{\mathbf{B}}\right) = \frac{1}{\mathbf{B_n}} - \frac{1}{\mathbf{B_{n+1}}} = \frac{2\pi}{\phi_0 S_{extr}}. \tag{2.21}$$

Here only extremal orbits on the Fermi-surface perpendicular to $\mathbf{B}$ with area S_{extr} are taken into account. Why this is the case will be discussed later. This determines the frequency

$$F = \frac{1}{\Delta(1/\mathbf{B})} = \frac{\phi_0}{2\pi}S_{extr} \tag{2.22}$$

at which the Landau-tubes cross the Fermi-level. As we consider the non-interacting case at $T = 0$, only states up to the Fermi-level are populated. This means that as the Landau-tube crosses the Fermi-level the states empty and cause a changes to the density of states at the Fermi-level. This periodicity is reflected in the heat-capacity, magnetization and other physical properties which are related to the density of states at the Fermi-level.

2.5.3 De Haas-Van Alphen Effect

The system which we are studying is best described by the temperature T, the volume V and the chemical potential μ. Therefor to study this system in more detail we will turn to the thermodynamic potential Ω. The magnetic moment of the system can be derived from Ω by the derivative

$$\mathbf{M} = -(\nabla_{\mathbf{H}}\Omega)|_{\mu=const}. \tag{2.23}$$

In order to obtain the thermodynamic potential for the Landau tubes of interest here, it is necessary to derive Ω at the previously determined energy levels (Eq. 2.19) and the degeneracy of each Landau tube. A detailed derivation of this can be found in reference [15]. At this point we will focus on the resulting expression for the thermodynamic potential and its implications on the magnetic moment.

The thermodynamic potential of electrons in a magnetic field is expressed as series over all harmonics p [15]

$$\Omega = \left(\frac{e}{2\pi\hbar}\right)^{3/2} \frac{e\hbar B^{5/2}}{m^*\pi^2} \left|\frac{\partial^2 S}{\partial k_z^2}\right|^{-1/2} \sum_{p=1}^{\infty} p^{-5/2} R_T R_D R_S \cos\left[2\pi p\left(\frac{F}{B} - \frac{1}{2}\right) \pm \frac{\pi}{4}\right]. \quad (2.24)$$

Following Eq. 2.23 we obtain the parallel magnetic moment

$$M_{\parallel} = -\left(\frac{e}{2\pi\hbar}\right)^{3/2} \frac{2Fe\hbar B^{1/2}}{m^*\pi} \left|\frac{\partial^2 S}{\partial k_z^2}\right|^{-1/2} \sum_{p=1}^{\infty} p^{-3/2} R_T R_D R_S \cos\left[2\pi p\left(\frac{F}{B} - \frac{1}{2}\right) \pm \frac{\pi}{4}\right]. \quad (2.25)$$

This formula is known as the *Lifshitz-Kosevich formula*. The component perpendicular to the field direction

$$M_{\perp} = -\frac{1}{F}\frac{\partial F}{\partial \theta} M_{\parallel}, \quad (2.26)$$

will be used later in the description of the torque magnetometery and should only be mentioned for completeness.

In the *Lifshitz-Kosevich* (LK) formula we find that the amplitude of the signal is altered by the second derivative of the cross-sectional area $|\partial^2 S/\partial k_z^2|^{-1/2}$. This is known as the *curvature factor*. In the case of an almost cylindrical Fermi-surface the variation of the orbits along the k_z direction will be very small in the vicinity of the extremal orbits. This will lead to the fact that the curvature factor will get large, therefore favour the observation of quasi-2-dimensional sheets of Fermi-surface rather than spherical sheets where the change along k_z is much larger. Physically this can be understood by imagining a Landau tube crossing the Fermi-surface in the case of a cylinder and in the case of a sphere. While for the cylinder in the case of $\mathbf{B} \parallel k_z$ all state suddenly empty at the same time, the Landau-tube empties continuously in the case of the sphere only leaving a small portion of the original state to empty at the extremal orbit.

The factors R_T, R_D and R_S describe damping of the quantum oscillation due to sample and material specific parameters. While there are more influences such as mosaic effects that can reduce the oscillation amplitude we will focus on these three main factors and discuss them in the next section.

2.5.4 Damping Factors

In the following we will discuss the the main damping factors influencing the oscillation amplitude. While the LK-formula was derived for a non-interacting electron gas the origin of the damping factor comes from many-body interaction and scattering mechanisms. However it can be shown that this does not influence the form of the LK-formula [16].

2.5.4.1 Finite Temperature

In the case of finite temperature the Fermi-Dirac distribution-function becomes smeared out. This has the effect that instead of a sudden depopulation of the Landau tubes when crossing the Fermi level the depopulation becomes smooth. In the case that the Landau-level spacing is smaller than the smearing $k_{\mathrm{B}}T$ of the Fermi-dirac distribution the depopulation of Landau tubes becomes continuous. As there is no sharp energy-level of depopulation anymore, we need to consider the contribution of a range of depopulation around the Fermi-level E_F. The change of $\mathrm{d}S/d\mathrm{E}$ within $k_{\mathrm{B}}T$ of the Fermi-level will, as we have seen in the previous section (Eq. 2.22), contribute a spectrum of frequencies. The superposition of these and their individual phases will cause a reduction in the oscillation amplitude. This reduction can be expressed as [15]

$$R_T = \frac{X}{\sinh(X)}, \tag{2.27}$$

with

$$X = \frac{2\pi^2 p k_{\mathrm{B}} T m^*}{e\hbar B} \approx 14.69 p m^* \frac{T}{B}. \tag{2.28}$$

The temperature dependence at constant magnetic field is entirely determined by the effective mass m^*. The reason for this can be seen when we combine the origin of the phase smearing $\mathrm{d}S/d\mathrm{E}$ with Eq. 2.16. At finite temperature the Fermi distribution leads to the population of a states around E_F. From this we find a distribution of frequencies that due to interference lead to a reduced spectral weight of the main frequency. For flat bands crossing the Fermi-level one finds large values of $\mathrm{d}S/d\mathrm{E}$ and hence a wide spread of frequencies. In order to observe a sharp peak in the oscillation spectrum one needs to go to much lower temperatures than for bands that have small variation of S around E_F.

We should keep in mind that the mass which will be determined using the temperature dependence of the dHvA-amplitude is renormalized by many-body interaction such as electron-electron and electron-phonon interaction over the band mass m_b.

The reason for the magnetic field entering Eq. 2.27 come from the spacing of Landau-levels. In the previous section we had found (Eqs. 2.15 and 2.20) that the Landau-level spacing is $\Delta E \propto B/m_c$. Hence the effect of phase-smearing will be reduced by higher magnetic fields as the spacing of Landau tubes will become larger. An example of the temperature damping is given in Fig. 2.5 for different effective masses in the range typically found in this work, and for a constant mass at different magnetic fields used in the current study of the iron-based superconductors.

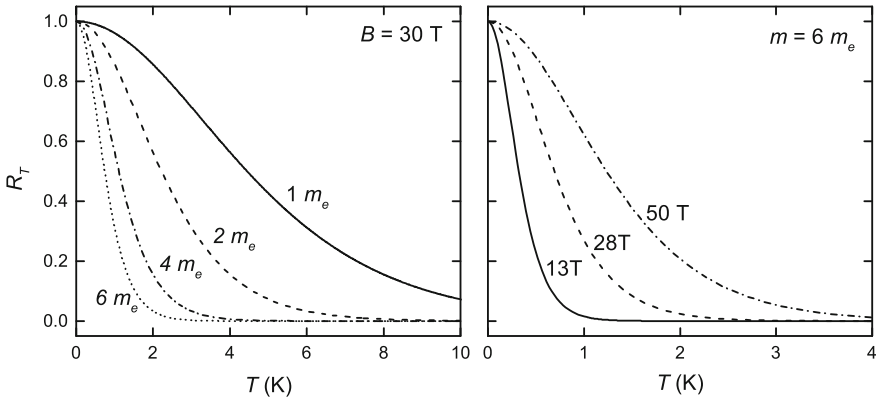

Fig. 2.5 The temperature damping term is plotted at $B = 30\,\mathrm{T}$ for different effective masses m^* (*left panel*) and for a constant effective mass $m^* = 6\,m_e$ at different magnetic fields (*right panel*)

2.5.4.2 Finite Lifetime

The effect of a finite life-time τ of the quasiparticle can be taken into account by introducing a Lorentzian broadening of the Landau-levels. The phase-smearing resulting from this effect is represented by [15]

$$R_D = \exp\left(\frac{p\pi}{\omega_c \tau}\right) \tag{2.29}$$

and is known as the *Dingle-term*. The expression in the exponent can also be expressed in terms of the mean free path l. For this we substitute ω_c using Eq. 2.15

$$\frac{\pi}{\omega_c \tau} = \frac{\pi m_c}{eB\tau}\frac{v_F}{v_F} = \frac{\pi}{eB}\frac{\hbar k_F}{l}, \tag{2.30}$$

where we used $\tau = v_F l$. By assuming a spherical orbit and Eq. 2.22 we can simplify this expression further

$$\frac{\pi}{eB}\frac{\hbar k_F}{l} = \frac{\hbar\pi}{e}\sqrt{\frac{2e}{\hbar}}\frac{\sqrt{F}}{lB} \approx \frac{1140\sqrt{F}}{lB}. \tag{2.31}$$

The mass, which enters the Dingle term, m_c, is not the renormalized mass that was found for the effective mass. It was derived theoretically by Wassermann et al. [17] and experimentally proven by Harrison et al. [18] that the mass used in the Dingle term is the band-mass m_b which can be found by band-structure calculation and only includes the renormalization due to the ionic lattice of the system [16]. We can also understand this by comparing the origin of the phase smearing in the two scenarios. While for the temperature damping term the distribution function is modified at finite

temperature, in the case of a finite life time the Landau levels are broadened. Many-body effects like electron-phonon coupling, effecting the dispersion relation $E(k)$ at E_F, hence enhance the effective mass measured in R_T, but keep the Landau level spacing, determined by ω_c, constant. This holds that the field dependence and hence the mean free path is unaffected by the many body interactions.

2.5.4.3 Spin Factor

In a paramagnetic system the electron-bands originating from spin-up and spin-down electrons are degenerate in zero field. This degeneracy is lifted under the influence of a magnetic field by Zeeman-splitting with an energy-difference of $\Delta E = g\mu_B B$, with the Bohr magneton μ_B and the gyromagnetic ratio g.

This leads to a phase-smearing influenced by the spin-mass m_S of the system, which is related to the Pauli-susceptibility that is not enhanced by electron-phonon interaction. Hence it differs from the effective mass determined by the temperature dependence.

The damping-factor can be calculated as [15]

$$R_S = \cos\left(\frac{p\pi g}{2}\frac{m_s}{m_b}\right). \tag{2.32}$$

The spin factor can lead to so call *spin-zeros*. Those are regions in the angle dependence for which the field-direction causes the split energy levels to be different by one flux-quantum, which cause a destructive superposition. However one has to be careful not to mistake these spin zeros with geometric zeros in the angle dependence caused by superposition of different extremal orbits. Those effects were for example found in $Tl_2Ba_2CuO_{6+\delta}$ [19].

2.5.4.4 Extremal Orbits

As mentioned before the observed quantum oscillations originate only from extreme cross-section-areas perpendicular to the applied field. This powerful tool, which allows us to map the topology of the observed quantum oscillation shall be discussed in a bit more detail, as it might not be clear at first sight why this is the case. We will assume a Fermi-surface which varies as $k_\perp = cos(k_\parallel)$, where $k_\parallel$ refers to the direction parallel to **B**. Using Eqs. 2.22 we will find a distribution of frequencies along $k_\parallel$. However, while most of these frequencies correspond to a smooth variation of the electron motion along $k_\parallel$ a strong effect in the energy of the system is observed where $\mathrm{d}F(k_\parallel)/\mathrm{d}k_\parallel$ is minimal and hence large sections of Landau tubes empty. This criteria describes the extremal orbits on the Fermi-surface.

An alternative way to find this result is to assume the frequency distribution $F(k_\parallel)$ which we already introduced. The expected signal can be calculated by

$$M = \int sin\left(2\pi \frac{F(k_\parallel)}{B}\right) \mathrm{d}k_\parallel. \tag{2.33}$$

The integral has to be carried out over the entire frequency distribution and phase smearing. This then gives the already known result that the signal only contains significant contributions form the extremal orbits.

2.6 Drude Model—Electronic Transport

The *Drude model*, which was the first to describe transport of electrons in metals, models the electrons as classical particles that follow Newton's law of motion

$$m\frac{d\mathbf{v}}{dt} = e\mathbf{E} - \frac{m}{\tau}\mathbf{v}, \tag{2.34}$$

for an electron of charge e in a electrical field E. The second term on the right hand side represent the friction that an electron experiences. The factor $1/\tau$ is of phenomenological nature, seen as strength of the friction whose microscopic origin is not specified. The differential equation holds two solutions. The homogeneous one $\upsilon \propto exp(-t/\tau)$, which shows that in absence of an electrical field the electron velocity decays exponentially. The factor τ is therefore seen as a mean life time. For the inhomogeneous differential equation at $t \gg \tau$ we obtain a constant velocity

$$\mathbf{v} = \frac{e\tau}{m}\mathbf{E}, \tag{2.35}$$

which is proportional to the external field E. From this we find for the current density

$$\mathbf{j} = ne\mathbf{v} = \frac{ne^2\tau}{m}\mathbf{E} = \sigma\mathbf{E}, \tag{2.36}$$

where we have used Ohms law in the last step. We see that the electrical conductivity σ of a metal is expected to be proportional to the carrier concentration and life time. The mean life time of a carrier is similar to the scattering time that we found in the description of the dHvA effect. While for the measurements of quantum oscillations samples with large τ as found from the residual resistivity $\sigma^{-1}(T = 0)$ are beneficial, the two values are not identical. The scattering rate τ in conductivity is mainly dominated by large angle scattering, while the values found in the Dingle term in dHvA include all types of scattering [15].

We will now include an external magnetic field, which alters the movement of the electrons and forces them on spherical orbits as already discussed in Sect. 2.5.1. The equation for the movement of the electrons is then given by

$$\frac{d\mathbf{v}}{dt} = \frac{e}{m}\mathbf{E} + \frac{e}{m}\mathbf{v} \times \mathbf{B} - \frac{1}{\tau}\mathbf{v}. \tag{2.37}$$

We chose to apply the magnetic field along the z-axis $\mathbf{B} = (0, 0, B_z)$. In the presence of a magnetic field the conductivity now given by a tensor as the magnetic field breaks the symmetry of the system. The conductivity tensor is given as

$$\sigma = \frac{ne^2\tau}{m} \begin{bmatrix} \frac{1}{1+\omega_c^2\tau^2} & \frac{\omega_c\tau}{1+\omega_c^2\tau^2} & 0 \\ -\frac{\omega_c\tau}{1+\omega_c^2\tau^2} & \frac{1}{1+\omega_c^2\tau^2} & 0 \\ 0 & 0 & 1 \end{bmatrix}, \tag{2.38}$$

with the cyclotron frequency $\omega_c = eB/m$. In the limit of very high magnetic field or high purity samples we find $\omega_c\tau \gg 1$, which leads to

$$\sigma_{xy} = \frac{ne}{B} \tag{2.39}$$

for the transverse conductivity known as *Hall conductivity* and

$$\sigma_{xx} = 0 \tag{2.40}$$

for the longitudinal conductivity. While the result found for the Hall effect is in agreement with experiments the vanishing conductivity is not verified in experiments.

To solve this problem we need to consider a system with two different carriers. This can be realized by assuming different effective masses, charges or scattering times. In this model one now finds that the total current $\mathbf{j}$ contains parts from both carriers

$$\mathbf{j} = \sigma_1\mathbf{E} + \sigma_2\mathbf{E}. \tag{2.41}$$

Therefore we obtain a change of resistivity due to the presence of a magnetic field [6]

$$\Delta\rho = \frac{\rho(B) - \rho(0)}{\rho(0)}. \tag{2.42}$$

For clean systems we find that where the residual resistivity $\rho(T = 0)$ becomes small the magnetoresistance increases. In a single band system this scenario can be realized by a k dependent effective mass or Fermi velocity.

2.7 Superconductivity

It took almost 50 years from the discovery of superconductivity by Kermlingh Onnes until the first microscopic understanding given by Bardeen, Cooper and Schrieffer (BCS). On the way to this theory a number of attempts for the description of this new ground state of electrons in a solid were made. In this section we will follow this path and start by the phenomenological thermodynamic treatment of the London brothers. From their work the *London penetration depth* is derived that describes the Meissner effect, where an external magnetic field is expelled from the bulk of the superconductor. We will then turn to the Ginzburg-Landau theory, which deals with the upper and lower limiting fields of superconductors based on Landaus theory of phase transitions. Finally we will end at the BCS theory which up to now is our best microscopic understanding of superconductivity. On the way we will focus and discuss those physical properties that will later be important in the analysis and understanding of experimental results.

2.7.1 London Penetration Depth

The London-penetration depth was first expressed by the London-brothers in their phenomenological work on the thermodynamics of superconductivity [20]. It describes the length-scale on which a magnetic field goes to zero inside a superconductor.

We start by assuming that for $T < T_c$ a portion of the total carrier density n has condensed to form the superconducting carrier density n_s. We can describe their motion analogue to the previous section

$$m\dot{\mathbf{v}}_\mathbf{s} = -e\mathbf{E}, \tag{2.43}$$

where we neglected the last term of the Drude-model as we assume the mean scattering of the electrons to go to infinity for a perfect conductor. By substituting $\mathbf{v_s}$ with the current density $\mathbf{j_s} = -n_s e\mathbf{v_s}$, we come to the conclusion that unlike in Ohms-laws, where the current density $\mathbf{j}$ is proportional to the electric field $\mathbf{E}$, here the time-derivative of j_s is proportional to $\mathbf{E}$. This leads to the fact that for a direct current there will be no potential difference over the sample. By using Maxwells-equation $\nabla \times E = -\partial B/\partial t$ we can transform Eq. 2.43 to

$$\frac{\partial}{\partial t}\left(\nabla \times \mathbf{j} + \frac{n_s e^2}{m}\mathbf{B}\right) = 0. \tag{2.44}$$

While this expression is valid for all conductors with the scatting time $\tau \to 0$, in the Meissner state the flux is zero in the static case. Hence for a superconductor in the Meissner state the expression in the brackets must be zero. This then gives the *London-equation*

$$\nabla \times \mathbf{j} + \frac{n_s e^2}{m}\mathbf{B} = 0. \tag{2.45}$$

By applying this equation to find out how the magnetic field changes upon entering a superconductor we find that it decays exponentially

$$B(x) = B_0 e^{-x/\lambda_l}, \tag{2.46}$$

inside the sample, with the characteristic length-scale

$$\lambda_L = \sqrt{\frac{m^*}{\mu_0 n_s e^2}}, \tag{2.47}$$

the *London-penetration depth*. Two things are important to notice. First the value of the London penetration depth is proportional to the superconducting carrier density in the limit of $T = 0$. This means that since most metals have similar charge carrier densities they will also possess similar penetration depth values only normalised by the effective mass m^* of the relevant system. Further at the superconducting critical temperature T_c n_s goes to zero and hence the penetration depth diverges. Secondly, as mention, the penetration depth of a superconductor, even at $T = 0$, depends on the normal state property m^*.

An alternative approach to derive the London penetration depth is from the finite frequency Drude model

$$\sigma(\omega) = \frac{ne\tau^2}{m}\frac{1}{1 - i\omega\tau}. \tag{2.48}$$

The integral over all real-part frequency is conserved and gives $\omega_p^2 = \pi ne^2/m$, the *plasma-frequency* ω_p, which is independent of the scattering rate. By taking the Drude model in the limit of $\tau = \infty$ we obtain the conductivity for the ideal conductor, that we can use with $j = \sigma E$ in the above expression and obtain the same result for λ_L, which we could also write as

$$\lambda_L^2 = \frac{\pi}{\mu_0 \omega_p^2}. \tag{2.49}$$

As the conductivity σ is also given as integral over the Fermi surface $\sigma \propto \int v_x^2 v_F^{-1} dS$ [21] we can link the penetration depth to this and find $\lambda_L^{-2} \propto \int v_x^2 v_F^{-1} dS$. This shows that the London penetration depth is dominated by sections of the Fermi surface where the Fermi velocity v_F is high and hence the effective mass is low.

2.7.2 Ginzburg-Landau Theory

The Ginzburg-Landau (GL) theory is a powerful tool as a first attempt to explain new experimental results in superconductors. Its macroscopic description from a thermodynamic viewpoint provides the possibility to explain systems without an exact microscopic understanding and can therefore hold more general results than a microscopic theory.

Ginzburg and Landau based their theory on the Landau-theory of phase-transitions. It starts from the view-point of the enthalpy of a system with an order parameter ψ which is zero above a critical temperature T_c, non-zero below and one at $T = 0$. Unlike the Landau-theory of phase-transitions where the order-parameter is real and constant in space, in the GL-theory the order parameter is given by the macroscopic superconducting wave-function $\psi(r) = \psi_0(r)\exp[-i\phi(r)]$. This is of complex nature and does not necessarily need to be constant in space. As the enthalpy is real we need to take the absolute value of the complex wave-function, which represent the density of superconducting particle $|\psi|^2 = n_s$. We then develop in terms of n^2. Taking this ansatz the GL-theory is strictly only valid close to T_c where $n_s \to 0$. In the vicinity of T_c the enthalpy per unit volume g is then given by

$$g_s = g_n + \alpha|\psi(r)|^2 + \frac{1}{2}\beta|\psi(r)|^4 + \frac{1}{2\mu_0}|B_a - B_i|^2 + \frac{1}{2m_s}|(i\hbar\nabla - e_s\mathbf{A})\psi(r)|^2, \qquad (2.50)$$

with the superconducting g_s and normal-state g_n enthalpy-density and the charge e_s and mass m_s of the superconducting wave function ψ. The last therm of Eq. 2.50 represents the kinetic energy of the Cooper pair due to an external magnetic field presented by the vector-potential $\mathbf{A}$. The second last is the displacement energy need to reduce the applied magnetic field B_a to zero inside the superconductor B_i in the Meissner-state. Since derived from a purely thermodynamic standpoint without any knowledge of the microscopic origin, this is probably the most general theory we have on superconductivity. However we will see in Sect. 4.3, where we discuss the upper and lower critical field, that for quantum critical systems, even this most general form fails.

2.7.2.1 Upper Critical Field

In addition to the London penetration depth λ, the GL theory predicts a second characteristic length scale of a superconductor, the GL coherence length ξ. This is derived in the zero field limit to [22]

$$\xi = \sqrt{\frac{\hbar}{4m|\alpha|}}. \qquad (2.51)$$

While α is unknown in this phenomenological approach a more precise formulation of ξ is found in BCS theory. Ginzburg and Landau realised that for $\kappa = \lambda/\xi > 1/\sqrt{2}$ the systems can lower their energy in field by allowing additional superconducting-

normal conducting interfaces. This causes the so call vortex-state between the lower and upper critical field and leads to higher critical fields were the material shows a finite resistivity. Using the GL-formalism we can determine this upper critical field H_{c2} at which the $g_s = g_n$. It can be shown [22] that this is the case for

$$\mu_0 H_{c2} = \frac{\Phi_0}{2\pi\xi^2(T)}. \tag{2.52}$$

The GL coherence-length ξ represents the length-scale at which the superconducting wave-function can vary from $\psi = 0$ to $\psi = \psi_\infty$. The criteria of $\psi = 0$ is fulfilled in the vortex core of a type-II superconductor in the mixed state. With this we can identify ξ as the vortex-core radius and H_{c2} as the field at which the normal-state vortex-cores start to overlap. Energetically speaking H_{c2} marks the magnetic field at which the kinetic energy of the screening currents exceeds the condensation energy $g_n - g_s$. This is also known as the orbital limiting effect. The Cooper pairs could also be broken due to the alignment of the spins in the applied magnetic field. This is known as the Pauli limiting field.

2.7.2.2 Lower Critical Field

The lower critical field H_{c1} of a type-II superconductor is the magnetic field at which the Gibbs-free energy of a Abrikosov vortex inside or outside the sample is equal [22]. For this we need the energy of a vortex line per unit length [22]

$$\epsilon_1 = \frac{H_{c1}\Phi_0}{4\pi}. \tag{2.53}$$

Inside the vortex the superconducting gap goes to zero and we find a normal state core. As in GL theory we describe the superconducting state with the complex function ψ, which varies at the superconducting-normal conducting interface like $|\psi| \approx \psi_\infty \tanh \frac{r}{\xi}$ [22]. In the case of a vortex we can therefore identify the parameter ξ as the core radius. The presence of a single flux $\phi_0 = h/2e$ causes screening currents that lead to a field profile [22]

$$h(r) \approx \frac{\phi_0}{2\pi\mu_0\lambda} \ln\frac{\lambda}{r}, \tag{2.54}$$

in the limit of $\lambda \gg \xi$ for $\xi \ll r \ll \lambda$. This would cause a divergent behaviour, which is cut off at $r \approx \xi$, the core radius. The vortex line energy can the also be expressed as the contribution form the field energy h and the kinetic energy of the shielding currents

$$\epsilon_1 \approx \left(\frac{\Phi_0}{2\pi\lambda}\right)^2 \ln\kappa. \tag{2.55}$$

In the derivation of this expression the core has been neglected. We find that the energy of a vortex line per unit length is inverse proportional to λ^2. By combining Eqs. 2.53 and 2.55 we obtain

$$H_{c1} \approx \frac{\Phi_0}{4\pi\mu_0\lambda^2} \ln \kappa \tag{2.56}$$

for the lower critical field. To account for the vortex core contribution that was neglected in the derivation a constant correction factor is used such that we find the result for lower critical field [22]

$$H_{c1} \approx \frac{\Phi_0}{4\pi\mu_0\lambda^2} \left(\ln \kappa + \frac{1}{2} \right) \tag{2.57}$$

2.7.3 BCS Theory

The first successful microscopic understanding of superconductivity was published by Bardeen, Cooper and Schrieffer (BCS) [23]. It had been shown by Fröhlich [24], that when electrons are placed inside a crystal most of the repulsive nature of the Coulomb interaction is screen. By assuming a simple screening model like the Thomas Fermi model we can limit the repulsive behavior to short range interactions. Further Fröhlich showed that it is possible for the electrons to develop an attractive interaction if one includes interactions with the lattice. Cooper then argued that by taking two electrons at $T = 0$ and placing them just above the Fermi level one can obtain a bound state which is energetically more favorable than having the electrons just above the Fermi-level [25]. This bound state is known as a *Cooper pair*. Built on Fröhlich's result that the electrons can interact via the lattice, only electrons of order $\hbar\omega_D$ were included (ω_D is the Debye-frequency). Using the necessary conservation of momentum one finds that the lowest energy state appears for $k_1 = -k_2$ where k_1 and k_2 are the wave-vectors of the interacting electrons. Hence the wavefunction is symmetric under spatial inversion restricting the spin part to be antisymmetric. The Cooper pairs therefore represent a singlet state.

Using the Cooper-pairs as a basis, BCS constructed a wavefunction to describe all electrons in the system. Without going into too much detail the main results of the BCS-theory shall be presented here.

Its was found that the energy of an elementary excitation can be expressed as [22]

$$E_{\mathbf{k}} = \sqrt{\epsilon_{\mathbf{k}}^2 + \Delta_{\mathbf{k}}^2} \tag{2.58}$$

with the normal state energy ϵ and the self-consistent expression for the energy gap

$$\Delta_{\mathbf{k}} = -\sum_{\mathbf{k}'} V_{\mathbf{k}\mathbf{k}'} \frac{\Delta_{\mathbf{k}'}}{2E_{\mathbf{k}'}}. \tag{2.59}$$

The BCS-theory assumes that the interaction potential V is constant and negative (attractive) for all $\mathbf{k}$ and hence results in a constant energy gap Δ. However in the *high-T_c* materials that are discussed in this thesis this is not the case and hence the more general form including the $\mathbf{k}$-dependence has been used.

Further the BCS-theory gives a result for the coherence length ξ which we had already discussed in the Ginzburg-Landau theory. Here the coherence length can be calculated as

$$\xi = \frac{\hbar v_F}{\pi \Delta}. \tag{2.60}$$

It now represents the length-scale, spacial extend, of a Cooper-pair.

The superconducting phase transition at T_c in zero field is is of second order, showing a jump of the heat capacity. The size of the anomaly in the heat capacity was determined in the BCS-theory for a *s*-wave superconductor in the weak coupling limit to be

$$\Delta C = 1.43 \gamma T_c, \tag{2.61}$$

where γ is the normal state Sommerfeld-coefficient which describes the electronic contribution to the heat capacity and is related to the effective mass via the density of states [26]

$$\gamma = \left(\frac{\pi k_b^2 N_A a^2}{3\hbar^2} \right) m^*. \tag{2.62}$$

2.8 Phase Transition

Understanding the emergence of new phases and their origin has been or great interest for a long time. We can best understand phase-transitions by turning to thermodynamics. In this work the energy of a system will be described using the Gibbs-free-energy G as it depends on temperature T and magnetic field B, which are typical parameters varied in the lab. Here we hold the particle number. and hence the chemical potential, constant. We assume that a system undergoes a phase-transition as function of the external parameter T. The point at which the phase transition occurs is determined by the relation $G(T < T_c) = G(T > T_c)$, where T_c is the critical point. Within the Landau-theory of phase transitions [1] we find that the transition can be of different order n. Following the classification of Ehrenfest the order of a phase transition is given by the lowest derivative of the free energy with respect to a thermodynamic parameter that is not continuous. If the order parameter, which is the first derivative with respect to the external field, is discontinuous than the phase transition is of first order. However for a continuous order parameter the phase transition is of higher order. This classification fails in the case of divergent order parameter at the phase

transition such as in ferro-magnetic materials. In modern physics we therefore distinguish between first-order phase transition, characterised by a latent heat involved in the transition, and second-order or *continuous* phase transitions which are characterized by a divergent fluctuations. In the transition that will be of interest for us and were discussed by Landau are of the second type.

In this case the phase transition is characterized by a continuous thermodynamic quantity m known as the *order parameter*, which is zero in the disordered state and then increases to reach one in the zero-temperature limit. While the average over the sample in the disordered state is zero, this does not rule out fluctuations of the order parameter. Those fluctuation possess a coherence length ξ which at T_c goes to infinity. We can express this in the form

$$\xi \propto |t|^{-\nu}, \tag{2.63}$$

with the dimensionless parameter $t = |T - T_c|/T_c$ and the critical exponent ν. While in this notation fluctuations are treated as spacial variations, when considering systems in quantum field theory, one treats them quasi-classical in d+1 dimensions, where the additional dimension is the imaginary time scale. For the fluctuation in time a typical life-time τ_c is given by

$$\tau \propto \xi^z \propto |t|^{-\nu z}. \tag{2.64}$$

Following these criteria we find for $T > T_c$ a disordered state with dynamic fluctuations of the order parameter and long-range static order of m for $T < T_c$. Hence we call ν the *correlation length critical exponent* and z the *dynamic critical exponent*.

We now considered the energy $\hbar\omega_c$ of the fluctuations, which we compare to the thermal excitation $k_B T$ of the system if T_c is finite. For a finite life-time of the excitations we find that

$$\omega_c \propto \tau_c^{-1} \propto |t|^{z\nu}. \tag{2.65}$$

For the case where $\hbar\omega_c << k_B T$, which can be rewritten as

$$|T - T_c| < T_c^{-z\nu} \tag{2.66}$$

the system can be treated classical [27]. However as $T_c \to 0$ this is not the case anymore and hence the description of the critical behavior close the critical point must take quantum mechanical effects into account. Therefore these phase transitions are called *quantum phase transitions* (QPT) and the point at which the order parameter goes to zero is called a *quantum critical point* (QCP). Also from the comparison of the energy levels we find that in the vicinity of a QCP a region exists where $\hbar\omega_c \geq k_B T$ and hence the properties of the system are governed by the fluctuations and quantum mechanics.

Before going into detail we should point out how a continuous phase transition appears in experiments. For this we will consider the heat capacity. As mentioned before the order parameter m is zero in the disordered state and changes continuously in the ordered state from zero. Therefore we can perform a Taylor expansion at $T = T_c$ of the Gibbs-energy

$$G(m,T) - G(0,T) = \frac{1}{2}am^2 + \frac{1}{4}bm^4 + ..., \tag{2.67}$$

which is valid for small m. Also we only consider the case where $G(m) = G(-m)$, hence systems that do not break time reversal symmetry, like magnetic systems in an external field. By taking the second derivative $T\partial_T G$ we obtain the expression for the heat capacity

$$C_V(m,T) - C_V(0,T) = \begin{cases} Ta^2/b & T < T_c \\ 0 & T > T_c \end{cases}. \tag{2.68}$$

We see that for a continuous phase transition the heat capacity has a jump at T_c. Remember this is a mean-field treatment and does not include any fluctuations of the order-parameter in the disordered state. By including those fluctuations one obtains the Gibbs-energy in the form $G[m((r),\tau),T]$, which is now a functional of the order parameter. To solve this one needs to find the partition function of this ensemble. An example of this can be found in Ref. [28]. In the case of fluctuations of the order parameter the heat capacity takes the form

$$C \propto |T - T_c|^{-\alpha}. \tag{2.69}$$

Instead of a step at T_c, the heat capacity diverges when approaching the critical point. The exponent α is a characteristic *critical exponent*. Following the same derivation one can also find critical exponents for other observables which are all characteristic for a given class of phase transitions [27]. For the Gaussian approximation the exponent α can be written as $\alpha = 2 - d/2$ with the dimensionality d of the system [29]. However the Gaussian approximation only holds for not too big fluctuations. In general the form $\alpha = 2 - d\nu$ is found, known as *hyperscaling*.

2.8.1 Quantum Phase Transition

We will assume a system to have an ordered ground state below a critical temperature T_0. By tuning a non-thermal parameter g(pressure, magnetic field or chemical potential) it is possible to suppress T_0 to zero temperature (see Fig. 2.6). Following Eq. 2.66

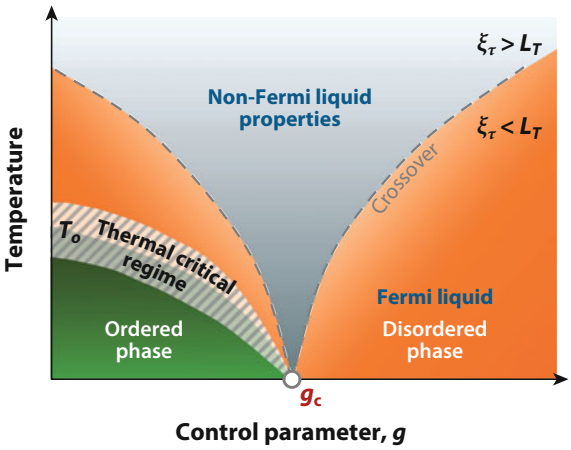

Fig. 2.6 Schematic phase diagram of a quantum critical point. Taken from Ref. [3]

we find that the region in which we can treat the critical behavior in the classical limit vanishes as we approach the QCP g_c. The only fluctuations available at this point to break the order are quantum fluctuations, resulting from Heisenberg's uncertainty principal. However, as we are experimentally not able to reach this point, we should raise the question: why is the appearance of a QCP important to the research conducted in this work? It was found in a variety of experiments that in the case of a QCP, physical properties such as transport, heat capacity and magnetic susceptibility differ from their typical behavior [3, 30]. While in most metals resistivity as a function of temperature is $\rho \propto T^2$, one finds $\rho \propto T^n$, with $n < 2$ in systems for $g = g_c$ (see for example Ref. [31, 32]). Quantum critical systems at finite temperature posses a finite length scale [33, 34]

$$L_\tau = \frac{\hbar c}{k_B T} \tag{2.70}$$

which limits the imaginary time axis for thermal fluctuations in two or more dimensions. As L_τ was given in the Heisenberg model c is the spin-wave velocity, specific to magnetic phase transitions. By comparing the length-scales Eqs. 2.64 and 2.70, two regimes emerge in the phase diagram for finite temperatures. For $L_\tau > \tau_c$ conventional behaviour, as described by Landau Fermi-liquid theory, is found. For the opposite case $L_\tau < \tau_c$ a *non-Fermi liquid* behaviour, as indicated in Fig. 2.6, evolves, which is found as typical v-shape region in the phase diagram using resistivity measurements [30, 32]. Also we conclude that in the low-temperature regime the excitations from the ground state are weakly affected by thermal fluctuation but relax on the much shorter quantum-time scale. In a mean field approach the system can therefore be explained by the ground-state wave-function. However starting at $g = g_c$ and going to high temperatures an increasing range of the phase diagram is

influenced by the quantum critical point, even for $g \neq g_c$. The appearance of this unusual part of the phase-diagram motivates interest in QCP and might be the reason for novel phases at finite temperature emerging from QPT.

References

1. L. Landau, Sov. Phys. JETP **3**, 920 (1957)
2. P. Coleman, A. Schofield, Nature **433**, 226 (2005)
3. T. Shibauchi, A. Carrington, Y. Matsuda, Annu. Rev. Condens. Matter Phys. **5**, 113 (2014)
4. S. Sachdev, Phys. Status Solidi B **247**, 537 (2010)
5. A. Schofield, Contemp. Phys. **40**, 95 (1999)
6. G. Czycholl, *Theoretische Festkörperphysik* (Springer-Verlag, Berlin Heidelberg, 2008)
7. G. Guiliane and G. Vignale, *Quantum Theory of the Electron Liquid*. Cambridge University Press (2005)
8. K. Capelle, Braz. J. Phys. **36**, 1318 (2006)
9. P. Blaha, K. Schwarz, G. Madsen, D. Kvasnicka, J. Luitz, *WIEN2K edited by Karl Heinz Schwarz* (Technische Universität Wien, Austria, 2001)
10. Z. Yin, K. Haule, G. Kotliar, Nat. Mater. **10**, 932 (2011)
11. J. Ferber, H. Jeschke, R. Valenti, Phys. Rev. Lett. **109**, 236403 (2011)
12. J. Ferber, K. Foyevtsova, R. Valenti, H. Jeschke, Phys. Rev. B **85**, 094505 (2012)
13. G. Kotliar, S. Savrasov, K. Haule, V. Oudovenko, O. Parcollet, C. Marianetti, Rev. Mod. Phys. **78**, 865 (2006)
14. L. Onsager, Philos. Mag. **344**, 1006 (1952)
15. D. Schoenberg, *Magnetic Oscillations in Metals* (Cambridge University Press, 1984)
16. M. Springford, *Electrons at the Fermi Surface* (Cambridge University Press, 1980)
17. A. Wasserman, M. Springford, Adv. Phys. **45**, 471 (1996)
18. N. Harrison, P. Meeson, P. Probst, M. Springford, J. Phys.: Condens. Matter **5**, 7435 (1993)
19. P. Rourke, A. Bangura, T. Benseman, M. Matusiak, J. Cooper, A. Carrington, N. Hussey, New J. Phys. **12**, 105009 (2010)
20. F. London, H. London, Proc. R. Soc. Lond. A **149**, 71 (1935)
21. M. French, Angle dependent magnetoresistance in $tl_2ba_2cuo_{6+\delta}$. Ph.D. dissertation, University of Bristol, 2009
22. M. Tinkham, *Introduction to Superconductivity* (Dover Publications, 1996)
23. J. Bardeen, L. Cooper, J. Schrieffer, Phys. Rev. **108**, 1175 (1957)
24. H. Fröhlich, Phys. Rev. **79**, 845 (1950)
25. L. Cooper, Phys. Rev. **104**, 1189 (1956)
26. N.W. Ashcroft, N.D. Mermin, *Solid State Physics*, 3rd edn. (Oldenbourg, 2007)
27. M. Vojta, Rep. Prog. Phys. **66**, 2069 (2003)
28. J. Annett, *Superconductivity* (Oxford University Press, Superfluids and Condensates, 2004)
29. S.-K. Ma, *Modern Theory of Critical Phenomena* (W.A. Benjamin Inc., 1976)
30. S. Sachdev, B. Keimer, Phys. Today **64**, 29 (2011)
31. S. Kasahara, K. Shibauchi, K. Hashimoto, K. Ikada, S. Tonegawa, R. Okazaki, H. Shishido, H. Ikeda, H. Takeya, K. Kirata, T. Terashima, Y. Matsuda, Phys. Rev. B **81**, 184519 (2010)
32. J. Custer, P. Gegenwart, H. Wilhelm, K. Neumaier, Y. Tokiwa, O. Trovarelli, C. Geibel, F. Steglich, C. Pepin, P. Coleman, Nature **424**, 524 (2003)
33. S. Sachdev, J. Ye, Phys. Rev. Lett. **69**, 2411 (1992)
34. A. Chubukov, S. Sachdev, J. Ye, Phys. Rev. B **49**, 11919 (1994)

http://www.springer.com/978-3-319-48645-1

Fermi Surface and Quantum Critical Phenomena of
High-Temperature Superconductors

Putzke, C.M.

2017, XV, 162 p. 104 illus., 23 illus. in color., Hardcover
ISBN: 978-3-319-48645-1